Quaternary Research 75 (2011) 91–103

Contents lists available at ScienceDirect

Quaternary Research

journal homepage: www.elsevier.com/locate/yqres

Marine radiocarbon reservoir effect along the northern Chile–southern Peru coast (14–24°S) throughout the Holocene

Luc Ortlieb [a,c,*], Gabriel Vargas [b], Jean-François Saliège [c]

[a] PALEOTROPIQUE, Institut de Recherche pour le Développement, 32 Avenue Henri Varagnat, 93143 Bondy Cedex, France
[b] Departamento de Geología, Facultad de Ciencias Físicas y Matemáticas, Universidad de Chile, Plaza Ercilla 803, Santiago, Chile
[c] LOCEAN, UMR 7159 (Université Pierre & Marie Curie, CNRS, IRD, MNHN), 4 place Jussieu, 75230 Paris Cedex 05, France

ARTICLE INFO

Article history:
Received 17 July 2006
Available online 19 September 2010

Keywords:
Radiocarbon reservoir effect
Holocene
Paleoceanographic circulation
Upwelling
Southeastern Pacific
Peru
Chile

ABSTRACT

Through an extensive sampling and dating of pairs of associated shells and charcoal fragments combined with reanalysis of all the available previous data, we reconstruct the evolution throughout the Holocene of the regional marine radiocarbon reservoir effect (ΔR) values along the northern Chile–southern Peru area (14°–24°S). After elimination of the cases in which the terrestrial component yielded older ages than the marine shells to which they were associated, the study is based upon data from 47 pairs of associated marine and terrestrial material.

Our results suggest major changes in both the magnitude and variability range of ΔR during the whole Holocene Period: (1) between 10,400 and 6840 cal yr BP, high values (511 ± 278 yr) probably result from a strengthened SE Pacific subtropical anticyclone and shoaling of equatorial subsurface waters during intensified upwelling events; (2) between 5180 and 1160 cal yr BP, lower values (226 ± 98 yr) may reflect a major influence of subtropical water and diminished coastal upwelling processes; (3) during the last ~thousand years, high values (between 355 ± 105 and 253 ± 207 yr) indicate an increased influence of ^{14}C-depleted water masses and of ENSO. For the early twentieth century a ΔR value of 253 ± 207 yr was calculated.

Introduction

The regional reservoir effect

Radiocarbon dating of marine biogenic carbonates involves estimates of the global marine reservoir effect (R) (Taylor, 1987) which has varied in time and space in response to global ocean-climate changes. This is partly due to oceanographic variations that reflect different ventilation rates of deep waters through time, changes in the input of ^{14}C-depleted dissolved inorganic carbon from deeper to surficial layers of the ocean and latitudinal variations of the concentration of radiocarbon in the ocean surface. Because at any geological time and even close to the ocean surface, the oceanic carbon is not in isotopic equilibrium with the atmospheric reservoir, radiocarbon measurements of marine materials tend to provide older apparent ages than contemporaneous terrestrial counterparts. Deep ocean water masses with low radiocarbon concentrations show that marine organisms may yield apparent ages that are older by several hundred years (up to 800–1000 yr) than their true age (Robinson and Thompson, 1981; Southon et al., 1990; Kovanen and Easterbrook, 2002). Global marine reservoir values at a decadal resolution have been estimated for the last roughly 22,000 yr from global models and the comparison of terrestrial and marine radiocarbon measurements, with a current R value estimated to ca. 400 yr (Stuiver et al., 1986; Stuiver and Braziunas, 1993). However, in most of the cases the marine correction may also incorporate an additional regional reservoir effect referred to as ΔR. This regional effect can reach particularly high values in high-latitude coastal zones and regions affected by strong upwelling processes. In coastal areas of tropical regions, upwelling systems bring ^{14}C-depleted waters to the sea surface and, subsequently, high regional reservoir effects are observed in marine organisms.

As the magnitude of the regional reservoir effect is related to ocean circulation changes and coastal upwelling regime, it has varied both through time and from one area to another one. Hence, in each study area, solving the problems of chronological correlation between radiocarbon results from marine and terrestrial samples requires that some assumption be made regarding the non-stationary, or permanent, value of ΔR. Testing whether the parameter ΔR varied in the past, or was different than modern ΔR values, may involve precise dating of coeval terrestrial and marine samples by independent methods based upon tephrachronology (e.g. Eiriksson et al., 2004) or cosmogenic and radiogenic measurements (Muscheler et al., 2000; van Beek et al., 2002). However, the most common method consists of comparing the results of radiocarbon analyses on contemporaneous terrestrial and

* Corresponding author. LOCEAN, UMR 7159 (CNRS, IRD, MNHN, Université Pierre et Marie Curie), Centre IRD France-Nord, 32 Avenue Henri Varagnat, 93143 Bondy Cedex, France. Fax: +33 148025554.
E-mail address: Luc.Ortlieb@ird.fr (L. Ortlieb).

0033-5894/$ – see front matter © 2010 University of Washington. Published by Elsevier Inc. All rights reserved.
doi:10.1016/j.yqres.2010.07.018

marine samples and inferring the ΔR values from the variation through time of the total marine reservoir R calculations (Head et al., 1983; Albero et al., 1986; Little, 1993; Southon et al., 1995; Ingram, 1998; Kennett et al., 1997; Phelan, 1999; Ulm, 2002).

Estimates of ΔR variation in time have been used for global paleoclimate reconstructions involving particular time periods, as the Last Glacial Maximum (Shackleton et al., 1988; Broecker et al., 1988; Sikes et al., 2000), the last deglaciation (Hughen et al., 1998; Kwiecien et al., 2008) or the Younger Dryas (Bard et al., 1994; Goslar et al., 1995; Muscheler et al., 2000; Kovanen and Easterbrook, 2002; Burr et al., 2009). In several regions of the world, the determination of former values of ΔR begins to play a major role in paleoceanographic studies concerned with circulation pattern and evolution of water masses (Angulo et al., 2007; Petchey et al., 2008; Fallon and Guilderson, 2008; Lewis et al., 2008; Ndeye, 2008; Burr et al., 2009).

Oceanographic setting and evidence for ΔR variation along southern Peru and northern Chile

The Humboldt Current System or Peru-Chile Current is affected by Eckman pumping and strong coastal upwelling activity driven by the upwelling-favorable equatorward winds associated with the south-eastern Pacific subtropical anticyclone (SEPSA), which drives southerly winds along the coast of central-northern Chile and southern Peru (Strub et al., 1998). The surficial components of this current transport subantarctic water equatorward and, in tropical and subtropical regions, subtropical water poleward (Strub et al., 1998). The subsurface Poleward Undercurrent (Strub et al., 1998) transports equatorial subsurface water (ESSW) to the south (Brandhorst, 1971; Morales et al., 1996) and below 500 m, the Antarctic intermediate water flows toward the equator (Fig. 1). The ESSW are ^{14}C-depleted (Toggweiler et al., 1991) and the shoaling of these water masses during strong coastal upwelling processes (Torres et al., 2002), certainly contributes to increasing the ΔR values in the northern Chile-southern Peru coastal region.

A modern ΔR value, measured on three pre-bomb mollusk shells of known age, was determined as 190 ± 40 yr (Taylor and Berger, 1967; Stuiver and Braziunas, 1993). This value was estimated from 20th-century samples and was later extrapolated to the last thousand years (Southon et al., 1995). However, older Peruvian archaeological sites provided marine shells which yielded radiocarbon apparent ages much older than coeval charcoal fragments (Rowe, 1965; Owen, 2002). This suggested that the regional reservoir effect probably fluctuated in the past and could have been significantly higher during some periods of the Holocene.

In an attempt to determine the ΔR value for the mid-Holocene (6–4 ka) in the region of Ilo (17°S, southern Peru), Kennett et al. (2002) generated a series of ^{14}C measurements of paired marine shells and charcoal fragments in a well-layered archeological site referred to as "Km 4" of a private railroad, north of Ilo. They observed that many pairs did not yield consistent age differences between mollusks and charcoal, and that some charcoal ages suggested anomalously old ages, by up to several centuries, with respect to contemporaneous marine shells. The anomalously old terrestrial samples reflect the fact that in the hyper-arid coastal environment of southern Peru (Schwerdtfeger, 1976), like other desert areas (Schiffer, 1986), early inhabitants probably used "old wood" fragments, either driftwood or dead trees which had ceased to live decades or centuries before they were used as fuel. This problem, of particular concern along coastal deserts, limits our ability to estimate ΔR values from comparisons of radiocarbon ages between marine shells and charcoal or wood fragments from archaeological sites.

In another study in the same region of Ilo, Owen (2002) dated pairs of marine and terrestrial materials in two small time windows (AD 1280–1380 and 1870–1680 BC). The terrestrial samples are small (1 to 3 mm in diameter) unburned twigs of *Schinus molle* (California pepper tree, or "*molle*") with bark which should not have been reworked, and hence should not present the "old wood" effect. Owen results indicated that ΔR had indeed varied, and much more than previously assumed by Southon et al. (1995). He concluded that if his and previous published results were accurate, there had been a considerable spatial/temporal variation of the regional reservoir effect in southernmost Peru.

More recently, Fontugne et al. (2004) reported differences of ^{14}C ages between marine shells and terrestrial organic materials from another Peruvian archaeological site (Quebrada de los Burros), near the Chilean border. These authors did not rely upon charcoal samples but on organic samples related to the meager vegetation which grew in the bed of a *quebrada* (dry-river talweg). In this case also, it can be assumed that the vegetation remains were most probably devoid of any "old wood" effect. They interpreted that the reservoir effect value increased ca.

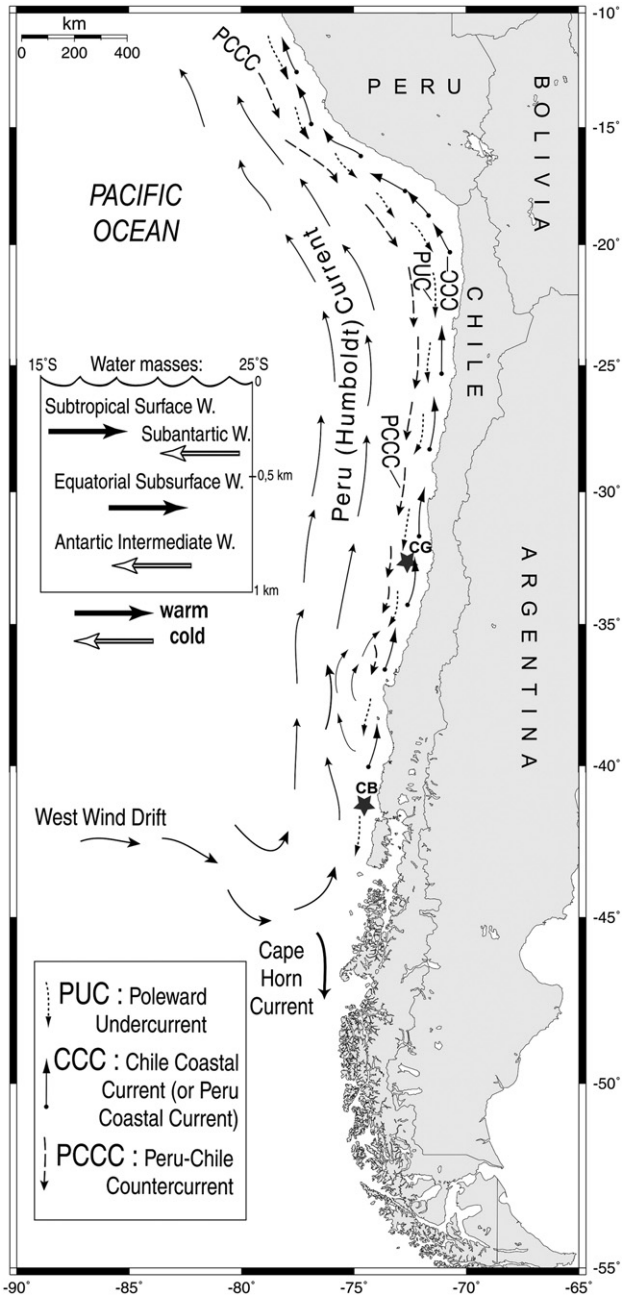

Figure 1. Regional oceanographic setting of the Peru-Chile study area, with major components of the Humboldt Current System during a typical summer situation (modified from Strub et al., 1998). Schematic sketch (inset) shows the disposition of the principal water masses. The location of sediment cores GIK17748-2 (CG) and GeoB3313-1 (CB), from Kim et al. (2002) and Lamy et al. (2002) are also shown.

8000 cal yr BP, stayed relatively high until ca. 4000 cal yr BP, and then decreased abruptly to a value comparable to the modern one. Fontugne et al. (2004) assigned these variations to probable fluctuations of the southern Peru coastal upwelling intensity and/or changes in ocean circulation at intermediate depth.

Recent studies on marine sedimentary sequences off northern and central Chile, documented significant upwelling and oceanographic variations at different time periods during the late Pleistocene and the Holocene (Marchant et al., 1999; Hebbeln et al., 2000, 2002; Kim et al., 2002; Lamy et al., 2004; Vargas et al., 2004; Dezileau et al., 2004). In fact, these paleoceanographic studies strongly suggest that the regional reservoir effect could have significantly varied in response to these ocean-climate variations. Based upon the analysis of new and previous radiocarbon data from a series of localities in the coastal southern Peru-northern Chile region, this work proposes: (1) to shed new light on significant ΔR variations at the scale of the last 11,000 yr, along a ~1000 km coastal stretch in the central part of the Humboldt Current System (14–24°S), and (2) to contribute to a better understanding of the relation between ΔR values, coastal upwelling regimes and regional oceanographic changes since the end of the Pleistocene.

Materials and methods

Sampling approach and methodological aspects

The estimation of the regional reservoir effect is based on a comparison between the radiocarbon composition of coeval materials which should reflect, at a given instant, the difference in the carbon isotopic composition of the atmospheric and marine reservoirs. In many cases, the materials used are pairs of marine shells and associated charcoal fragments, sampled either in isolated campfire remnants or in stratified archaeological deposits. In a few other cases (e.g. Fontugne et al., 2004), the dated materials may consist of thrown away marine shells associated with vegetation remains thought to be contemporaneous with the consumption of the marine resource. The approach implies that the contemporaneity of the marine and terrestrial dated samples can be firmly established, or at least reasonably assumed. Thus, in all such studies, there is not only a question of the chronological association of the samples, but also a question of the relative age of both components of the pair (e.g. the "old wood" effect of Kennett et al., 2002).

The close association between marine shells and charcoal or wood fragments can be reasonably assessed when they come from isolated campfire deposits, in which possible mixing of similar materials from younger or previous sedimentary layers can be ruled out. These situations, corresponding to short-lived occupation episodes left by nomadic populations, are relatively numerous in the coastal arid environment of southern Peru and northern Chile. When the paired samples come from archaeological sites occupied for centuries, special care has been taken to avoid material mixing from layers of different ages.

In a number of localities, available radiocarbon data may concern several samples of shells, or vegetal remains which are all contemporaneous. To form the pairs from which ΔR values are calculated, we distinguished two cases. When two (or more) radiocarbon measurements on charcoal samples were available, we discarded the result yielding the oldest apparent age, susceptible to reflect a possible old wood effect, and used only the youngest radiocarbon age. On the other hand, when radiocarbon data on two, or several, marine shell samples associated to a single dated charcoal were available, we considered these as several pairs. When radiocarbon measurements were available on several coeval shells, the data provide a useful indication on the variability range of ΔR in the corresponding nearshore environment at the given date. In Table 1, we identified pairs of samples by notation in the form 1–1, 1–2, etc., in which the first digit corresponds to the terrestrial sample and the second one to each associated marine sample.

All the shells analyzed in the study correspond to kitchen remains, and are thought to be organisms that were fished in the few hours (or days, at most) preceding their consumption by humans. The mollusc shells come from the nearshore environment (water depth which seldom exceeded 10 m) and can be considered as equivalently significant in terms of ^{14}C composition. No specific/generic differences were observed within the results. At an individual level, there are no arguments leading to consider that during their life time, the shell isotopic composition may have been affected by other phenomena than the variation of the composition of the dissolved carbon of the marine waters. Because of the general lack of estuaries, coastal lagoons, and continental runoff reaching the sea, we assume that no terrestrial influence affected the nearshore environment of the study area. In this respect, there is no reason to suspect that the radiocarbon composition of the marine shells, from any of the studied localities, reflects any continental impact (Dye, 1994; Phelan, 1999; Eiriksson et al., 2004).

Although most of the marine samples included here consist of calcium carbonate shells of invertebrate (mainly molluscan) organisms, we also used data from one previous study which includes feathers or sea-bird skin and fish vertebrae (Southon et al., 1995). The radiocarbon composition of soft parts of birds which feed exclusively on marine resources, or of fish, is considered to be equally reliable as marine mollusks.

Radiocarbon data from a few shells of known age and which grew before 1950 are also used for the evaluation of ΔR value. These samples, which lived in the first half of the 20th century, allow a direct determination of ΔR. Two gastropod shell samples (supposedly collected alive) provided the first evaluation of the reservoir effect in the study area (Taylor and Berger, 1967). One of them (*Oliva peruviana*), identified as from "southern Peru, 14°S, 78°W" (the indicated longitude is obviously wrong, and should read "76°W", because the locality was certainly near Pisco) was collected in the 1930s. The other sample, collected in 1925 in the Antofagasta area (24°S, 70°W), is a shell of the species *Concholepas concholepas* (Table 1).

We also included several shells collected in nitrate mining camps (*"salitreras"*) that were active at the end of the nineteenth century and the first decades of the twentieth century, and were subsequently abandoned. The refuse shells were collected in three *salitreras* that had been working during known, well-bracketed, periods. In Salitrera Slavonia (20°51'S, 69°42'W) and Salitrera Buenaventura (21°49'S, 69°44'W), active in the periods 1900–1918 and 1894–1930 respectively, we sampled *Protothaca thaca* shells. In Salitrera Prat (23°04'S, 69°29'W), active between 1912 and 1931, several individual samples of *Argopecten purpuratus* shells were collected and dated (Table 1). We assumed that the calendar age (cal yr BP) of each of these samples is the arithmetical mean of the occupation period of the *salitreras*, i.e.: 41 ± 9 yr BP for Salitrera Slavonia, 38 ± 18 yr BP for Salitrera Buenaventura, and 28.5 ± 9.5 yr BP for Salitrera Prat.

Analytical procedures

Most of the radiocarbon dating that we performed on marine and terrestrial samples was carried out at the LODYC (now renamed LOCEAN, for Laboratoire d'Océanographie et du Climat: Expérimentation et Analyses Numériques) facility (lab. ref. "Pa", Table 1) and the PALEOTROPIQUE laboratory (lab. ref. "PaBO", Table 1). Some radiocarbon data were obtained at the University of Toronto facility (Ottawa, Canada) (lab. ref. "TO", Table 1), the GEOTOP laboratory (Université of Québec at Montréal, Canada) (lab. ref. "UQ", Table 1) and the NSF Radiocarbon Facility (University of Arizona, Tucson, USA) (lab ref. "AA", Table 1). For data provided by previous authors, the reader is invited to refer to the original published works.

In most cases, the analyzed shell samples corresponded to whole shells (single shells in the case of large *C. concholepas* individuals, or

Table 1

Sampling site data and sample characteristics, with geochemical and radiocarbon results of associated marine (in grey) and atmospheric material within the study area, from new localities and previously studied sites (see Figs. 2 and 3). Only pairs which did not show anomalously old wood/charcoal ages with respect to marine sample radiocarbon data were actually used to estimate reliable ΔR values (10th column). Data in italics in columns 3 to 7 designate samples that were not considered as reliable, either because of old wood effect, or because of anomalous geochemical results ($\delta^{13}C$). Numbers in parentheses in the 8th column correspond to the amount of probability for the corresponding calibrated age range period. When radiocarbon data for two or more terrestrial samples were available in a given locality, it was the data of the youngest sample that was selected for the ΔR calculation. When data from charcoal and yarn samples were available, we chose the charcoal data, for consistency sake.

Site/Reference	Pairs	Type of material	Lab #	Field #	$\delta^{13}C$ (°/°°)	Terr. Cal. Age AD/cal yr BP / Conv. Marine Age, cal yr BP	Terrestrial Cal. Range cal yr BP*/ Terrestrial Cal. Mean cal yr BP	Conv.Mar. Age cal yr BP Curv. Min. Curv. Max.	Mean ΔR (yr)	Marine Δ ^{14}C (°/°°)
MODERN PRE-BOMB TWENTIETH CENTURY- SAMPLES										
Southern Peru: 14°0'S, 78°0'W										
Taylor and Berger (1967)						AD 1930–1940	(1.00) 10–20/ 15±5	**454±23** **460±23**		
	1.1	***Oliva peruviana***	**UCLA1279**		**1.2**	**1127±44**			**670±35**	**−132.9±5.3**
Antofagasta: 24°0'S, 70°0'W										
Taylor and Berger (1967)						AD 1925	(1.00) 25–25/ 25±0	**451±23** **451±23**		
	1.1	***C. concholepas***	**UCLA1277**		**0.1**	**626±34**			**175±29**	**−72.2±3.9**
Salitrera Buenaventura: 21°49'05"S, 69°43'40"W										
						AD 1894–1930	(1.00) 20–56/ 38±18	**448±23** **465±23**		
This work	**1.1**	***Protothaca thaca***	**Pa2250**	**C02-441**	**1.2**	**645±33**			**189±28**	**−72.9±5.8**
Salitrera Prat:: 23°04'00"S, 69°29'20"W										
						AD 1912–1931	(1.00) 19–38/ 28.5±9.5	**448±23** **454±23**		
This work	**2.1**	***Argopecten purpuratus***	**Pa 2055**	**C00-425a**	**1.6**	**540±60**			**89±45**	**−61.8±8.1**
id.	**2.2**	***Argopecten purpuratus***	**Pa 2057**	**C00-425b**	**1.7**	**795±30**			**344±27**	**−91.1±4.4**
id.	**2.3**	***Argopecten purpuratus***	**PaBO 32**	**C00-425c**	**1.2**	**474±32**			**23±28**	**−54.1±4.9**
id.	**2.4**	***Argopecten purpuratus***	**PaBO 33**	**C00-425d**	**1.1**	**598±29**			**147±26**	**−68.6±4.4**
id.		*Argopecten purpuratus*	*PaBO 50*	*C00-425e*	*2.8**	*956±46*				
id.		*Argopecten purpuratus*	*PaBO 51*	*C00-425f*	*2.5**	*706±30*				
Salitrera Slavonia: 20°50'43"S, 69°42'13"W										
						AD 1900–1918	(1.00) 32–50/ 41±9	**448±23** **454±23**		
This work	**3.1**	***Protothaca thaca***	**Pa 2268**	**C00-442**	–	**835±40**			**384±33**	**−94.2±5.5**
HOLOCENE (PRE-TWENTIETH CENTURY) SAMPLES										
Chala: 15°50'S, 74°18'W										
This work	**1**	Charcoal	PaBO4	P01-13	−18.3	720±72	(1.00) 544–728/ *636±92*			
id.		*Wood*	*PaBO26*	*P01-14*	*−18.9*	*1079±72*				
id.	**1.1**	*C. concholepas*	PaBO18	P01-12	−1.4	1080±64				
Panam. Km 737: 16°20'S, 73°19'W										
This work	**1**	Charcoal	PaBO6	P01-19	−11.6	7970±159	(0.98) 8403–9139/ 8771±368			
id.	**1.1**	*Mesodesma donacium*	PaBO25	P01-20	0.14	8184±84				
id.	**2**	Charcoal	PaBO5	P01-15	−14.2	7511±126	(0.99) 8006–8463/ 8235±229	**7563±30** **8017±26**		
id.	**2.1**	***Mesodesma donacium***	**PaBO24**	**P01-16**	**0.0**	**8255±88**			**465±65**	**−30.9±37.4**
id.	**3**	Charcoal	PaBO7	P01-17	−13.5	8892±132	(1.00) 9555–10203/ 9879±324	**8943±27** **9367±27**		
id.	**3.1**	***Mesodesma donacium***	**PaBO19**	**P01-18a**	**0.7**	**9334±159**			**179±114**	**33.7±61.0**
id.	**3.2**	*Mesodesma donacium*	PaBO45	P01-18b	0.4	9129±156				
id.	**4**	Charcoal	PaBO82	P03-45	−25.5	9564±103	(0.99)10551–11172/ 10862±311			
id.	**4.1**	*Mesodesma donacium*	PaBO81	P03-46	0.2	9402±41				
id.	**5**	Charcoal	PaBO83	P03-47a	−28.5	9152±42	(0.84)10187–10303/ 10245±58			
id.	**5.1**	*Fisurella sp.*	PaBO78	P03-47b2	0.5	9327±35				
id.	**6**	Charcoal	PaBO84	P03-49	−28.4	8983±52	(0.98) 9887–10226/ 10057±170			
id.	**6.1**	*Mesodesma donacium*	PaBO80	P03-48	0.5	9245±35				
Miraflores: 17°2'S, 71°23'W										
This work	**1**	Charcoal	PaBO85	P03-50	−26.5	8780±147	(1.00) 9495–10180/ 9838±343			
id.	**1.1**	Marine shell	PaBO77	P03-51	−1.1	8292±44				
S Pta Bombon: 17°14'S, 71°36'W										
This work	**1**	Charcoal	PaBO2	P01-21	−18.1	2238±108	(0.99) 1884–2366/ 2125±241	**2282±26** **2712±27**		
id.	**1.1**	***C. concholepas***	**PaBO23**	**P01-23**	**−0.3**	**2810±60**			**313±46**	**−88.5±33.4**

Table 1 (*continued*)

Site/Reference	Pairs	Type of material	Lab #	Field #	$\delta^{13}C$ (‰)	Terr. Cal. Age AD/cal yr BP / Conv. Marine Age, cal yr BP	Terrestrial Cal. Range cal yr BP*/ Terrestrial Cal. Mean cal yr BP	Conv.Mar. Age cal yr BP Curv. Min. Curv. Max.	Mean ΔR (yr)	Marine Δ ^{14}C (‰)
N Ilo: 17°19'S, 71°26'W										
This work	**1**	Charcoal	PaBO10	P01-24	−26.1	8367±85	(0.98) 9081–9487/ 9284±203			
id.		*Snails*	*PaBO13*	*P01-26*	*−8.4*	*8385±82*				
id.	**1.1**	*C. concholepas*	PaBO15	P01-25a	−0.3	8687±77				
id.	**1.2**	*C. concholepas*	PaBO58	P01-25b	−0.2	8664±116				
Pocoma: 17°25'S, 71°23'W										
This work	**1**	Charcoal	AA58004	P01-27	−27.1	1079±32	(0.9) 904–983/ 944±40			
id.		*Yarn*	*PaBO27*	*P01-29*	*−27.3*	*900±54*				
id.	**1.1**	*Choromytilus chorus*	PaBO21	P01-28a	1.6	1387±55				
id.	**1.2**	*Tegula sp.*	PaBO16	P01-28b	1.7	1405±76				
id.	**1.3**	*C. concholepas*	PaBO17	P01-30	−0.2	1337±59				
Loreto Viejo: 17°36'S, 71°14'W										
Owen (2002)	**1**	*Schinus molle*, others	Beta51073	Unit2505-5-6/ near top	−26.3	730±60	(1.00) 554–722/ 638±84	**986±25** **1186±25**		
id.	**1.1**	***Choromytilus chorus***	**AA37160**	**Unit2505-5-6/ near top**	**0.3**	**1358±46**			**272±37**	**−87.8±14.5**
id.	**2**	*Schinus molle*	AA37161	Unit2505-11-17/ near bottom	−27.7	701±38	(1.00) 559–667/ 613±54	**993±26** **1128±26**		
id.	**2.1**	***Choromytilus chorus***	**AA37162**	**Unit2505-11-17/ near bottom**	**0.4**	**1428±56**			**368±44**	**−98.4±12.2**
id.	**3**	*Schinus molle*	AA40291	Unit2503-6-6	−26.3	662±34	(1.00) 551–653/ 602±51	**977±25** **1085±25**		
id.	**3.1**	***Choromytilus chorus***	**AA40292**	**Unit2503-6-6**	**0.0**	**1530±40**			**499±33**	**−111.0±9.9**
id.	**4**	*Schinus molle*	AA37165	Unit2513-11-18/ near bottom	−26.7	3439±43	(0.97) 3478–3724/ 3601±123	**3602±26** **3797±26**		
id.	**4.1**	***Choromytilus chorus***	**AA37166**	**Unit2513-11-18/ near bottom**	**−0.1**	**3961±47**			**262±38**	**−55.8±19.6**
Tacahuay: 17°49'S, 71°07'W										
This work	**1**	Charcoal	Pa 1924	PS 39	−26.2	7970±130	(0.98) 8424–9036/ 8730±306			
id.	**1.1**	Marine shell	Pa 1943	PS40	0.3	8293±60				
id.	**2**	Charcoal	Pa 1907	PS 49	−25.5	9365±110	(0.99)10231–10786/ 10509±278			
id.		*Snails*	*Pa 1914*	*PS 51*	*−6.5*	*9345±100*				
id.	**2.1**	*Choromytilus chorus*	Pa1937	PS 50	−0.1	9065±125				
id.	**3**	Charcoal	Pa 1810	PS30	−26.4	9670±80	(1.00)10721–11196/ 10959±238			
id.	**3.1**	*C. concholepas*	Pa 1811	PS31	0.9	9986±80				
El Ahogado: 17°58'S, 70°53'W										
This work	**1**	Charcoal	Pa 1906	PS 35	−24.9	6065±70	(0.98) 6665–7023/ 6844±179	**6226±27** **6680±28**		
id.		*Charcoal*	*Pa 1776*	*PS 14*	*−24.4*	*6785±60*				
id.	**1.1**	***Chiton sp.***	**Pa 1784**	**PS 15**	**0.5**	**7505±60**			**1052±47**	**−100.8±26.2**
id.	**1.2**	***C. concholepas***	**Pa 1785**	**PS15'**	**0.0**	**7285±60**			**832±47**	**−75.9±26.9**
id.	**1.3**	***P. purpuratus***	**Pa 1786**	**PS15"**	**1.4**	**6885±60**			**432±47**	**−28.7±20.9**
id.	**2**	Charcoal	Pa 1789	PS16	−21.4	3660±40	(0.89) 3825–4005/ 3915±90			
id.	**2.1**	*C. concholepas*	Pa 1790	PS17	0.4	3695±40				
id.	**3**	Charcoal	Pa 1768	PS3	−25.0	3535±60	(1.00) 3579–3903/ 3741±162	**3674±26** **3929±25**		
id.	**3.1**	***P. purpuratus***	**Pa 1792**	**PS4**	**1.7**	**4145±60**			**344±46**	**−61.4±25.4**
id.	**3.2**	***Chiton sp.***	**Pa 1791**	**PS4'**	**1.1**	**3865±60**			**64±46**	**−28.2±26.3**
id.	**4**	Charcoal	Pa 1769	PS5	−22.6	3515±40	(0.99) 3613–3843/ 3728±115	**3698±26** **3880±27**		
id.	**4.1**	***P. purpuratus***	**Pa 1770**	**PS6**	**1.8**	**4115±60**			**326±46**	**−59.4±20.1**
id.	**4.2**	***Loxechinus albus***	**Pa 1773**	**PS7**	**−3.1**	**4035±60**			**246±46**	**−50.0±20.3**
Km 4-N Ilo: 17°32'11"S, 71°21'27"W										
Kennett et al. (2002)	**1**	Charcoal	CAMS1770	1c: Stratum V	–	4500±60	(0.65) 4873–5146/ 5010±137	**4685±26** **4841±25**		
id.	**1.1**	***C. concholepas***	**CAMS1744**	**1s: Stratum V**	–	**4950±50**			**48±36**	**−10.1±22.4**
id.	**2**	Charcoal	CAMS1770	9c: Stratum VII	–	4940±60	(0.83) 5568–5749/ 5659±91			
id.	**2.1**	*C. concholepas*	CAMS1744	9s: Stratum VII	–	4980±60				
id.	**3**	Charcoal	CAMS1770	8c: Stratum VIII	–	4940±60	(0.83) 5568–5749/ 5659±91			
id.	**3.1**	*C. concholepas*	CAMS1744	8s: Stratum VIII	–	4990±70				
id.	**4**	Charcoal	CAMS1770	7c: Stratum X	–	5020±80	(1.00) 5585–5906/ 5746±161			
id.	**4.1**	*C. concholepas*	CAMS1744	7s: Stratum X	–	4990±50				
id.	**5**	Charcoal	CAMS1772	2c: Stratum XII	–	4930±60	(1.00) 5468–5746/ 5607±139			
id.	**5.1**	*C. concholepas*	CAMS1745	2s: Stratum XII	–	4890±60				
id.	**6**	Charcoal	CAMS1772	3c: Stratum XIII	–	4620±60	(0.84) 5035–5333/ 5184±149	**4786±26** **5025±25**		
id.	**6.1**	***C. concholepas***	**CAMS1744**	**3s: Stratum XIII**	–	**5050±60**			**145±46**	**67.2±25.5**
id.	**7**	Charcoal	CAMS1783	6c: Stratum XVIII	–	5060±80	(1.00) 5600–5909/ 5755±155			
id.	**7.1**	*C. concholepas*	CAMS1744	6s: Stratum XVIII	–	5070±60				
id.	**8**	Charcoal	CAMS1770	4c: Stratum XXI	–	4940±60	(0.83) 5568-5749/ 5659±91			
id.	**8.1**	*C. concholepas*	CAMS1744	4s: Stratum XXI	–	5080±60				
id.	**9**	Charcoal	CAMS1770	5c: Stratum XXII	–	4530±80	(1.00) 4870–5312/ 5091±221	**4670±25** **4990±25**		
id.	**9.1**	***C. concholepas***	**CAMS1744**	**5s: Stratum XXII**	–	**4950±70**			**120±53**	**−0.3±35.4**

(*continued on next page*)

Table 1 (*continued*)

Site/Reference	Pairs	Type of material	Lab #	Field #	$\delta^{13}C$ (‰)	Terr. Cal. Age AD/cal yr BP / Conv. Marine Age BP	Terrestrial Cal. Range cal yr BP*/ Terrestrial Cal. Mean cal yr BP	Conv.Mar. Age cal yr BP Curv. Min. Curv. Max.	Mean ΔR (yr)	Marine Δ ^{14}C (‰)
Los Burros: 18°01'S, 70°50'W										
Fontugne et al. (2004)	**1**	Organic layer	GIF10648	QLB17	−15.0	3700 ± 40	(1.00) 3844–4088/ 3966 ± 122	**3880 ± 27 4066 ± 26**		
id.	**1.1**	**Marine shell**	**GIF10404**	**QLB17**	**0.3**	**4445 ± 40**			**472 ± 34**	**-70.9 ± 18.3**
id.	**2**	Organic layer	GIF10634	QLB3	−19.7	8040 ± 105	(1.00) 8550–9129/ 8840 ± 290	**8091 ± 26 8518 ± 27**		
id.	**2.1**	**Marine shell**	**GIF10401**	**QLB3**	**0.3**	**8780 ± 70**			**476 ± 53**	**71.0 ± 42.7**
id.	**2.2**	Marine shell	GIF11453	QLB23	0.0	8315 ± 60				
id.	**3**	Organic layer	GIF10633	QLB2	−15.0	8160 ± 70	(1.00) 8762–9282/ 9022 ± 260	**8241 ± 27 8612 ± 29**		
id.	**3.1**	**Marine shell**	**GIF10400**	**QLB2**	**-1.0**	**8860 ± 130**			**434 ± 94**	**-11.4 ± 47.1**
id.	**4**	Organic layer	GIF10645	QLB14	−13.6	6595 ± 75	(1.00) 7306–7575/ 7441 ± 135	**6782 ± 27 7105 ± 27**		
id.	**4.1**	**Marine shell**	**GIF10647**	**QLB16**	**0.7**	**7160 ± 80**			**217 ± 60**	**8.9 ± 26.5**
id.	**5**	Organic layer	GIF10640	QLB12	−15.3	7390 ± 50	(0.88) 8014–8221/ 8118 ± 104	**7578 ± 31 7762 ± 28**		
id.	**5.1**	**Marine shell**	**GIF10646**	**QLB15**	**0.5**	**8125 ± 30**			**455 ± 30**	**-28.9 ± 15.8**
id.	**6**	Charcoal	GIF99341	D9/2INF	−25.3	6090 ± 80	(0.86) 6715–7032/ 6874 ± 159	**6263 ± 29 6530 ± 28**		
id.	**6.1**	**Marine shell**	**GIF99509**	**D9/2INF**	**0.6**	**7070 ± 80**			**674 ± 60**	**-47.4 ± 27.8**
id.	**7**	Charcoal	GIF99576	E9/2Sup	−17.9	6560 ± 90	(1.00) 7261-7571/ 7416 ± 155	**6737 ± 27 7074 ± 27**		
id.	**7.1**	**Marine shell**	**GIF99510**	**E9/2Sup**	**0.6**	**7480 ± 80**			**575 ± 60**	**-33.4 ± 27.8**
id.	**8**	Charcoal	GIF10629	Cañon	−25.3	3120 ± 80	(0.98) 3058–3447/ 3253 ± 195	**3238 ± 26 3572 ± 25**		
id.	**8.1**	**Marine shell**	**GIF10722**	**Cañon**	**0.0**	**3595 ± 90**			**190 ± 66**	**-52.5 ± 32.9**
id.	**9**	Charcoal	GIFA100347	E5-6N4	–	6500 ± 80	(0.96) 7240–7506/ 7373 ± 133	**6702 ± 27 7016 ± 27**		
id.	**9.1**	**Marine shell**	**GIFA100348**	**E5-6N4**	–	**7790 ± 120**			**931 ± 87**	**-74.8 ± 28.7**
id.	**10**	Wood	GIF11457	QLB31	−22.9	375 ± 30	(0.98) 318–474/ 396 ± 78	**704 ± 23 833 ± 25**		
id.	**10.1**	**Marine shell**	**GIF11456**	**QLB31C**	**-0.5**	**1050 ± 30**			**282 ± 27**	**-79.5 ± 12.1**
id.	**11**	Charcoal	GIFA100142	DE9/fondN2	–	6090 ± 110	(0.99) 6636–7176/ 6906 ± 270	**6190 ± 26 6650 ± 30**		
id.	**11.1**	**Marine shell**	**GIF10649**	**N2a**	**-0.4**	**6640 ± 50**			**220 ± 41**	**8.9 ± 39.2**
id.	**12**	Organic layer	GIF10642	QLB11	-13.4	8650 ± 70	(1.00) 9462–9765/ 9614 ± 152	**8782 ± 28 9064 ± 27**		
id.	**12.1**	**Marine shell**	**GIF11452**	**QLB22**	**-0.1**	**9725 ± 90**			**802 ± 67**	**-46.4 ± 27.0**
id.	**13**	Charcoal	GIFA100343	B0C5/N4-5383	−16.5	7360 ± 100	(1.00) 7952–8342/ 8147 ± 195			
id.	**13.1**	Marine shell	GIFA100342	B0C5/N4-5383	−0.4	7880 ± 90				
id.	**14**	Charcoal	GIFA97289	A3NIV2B	−20.5	6630 ± 70	(0.90) 7411–7583/ 7497 ± 86			
id.	**14.1**	Marine shell	GIF10689	N2B	−0.2	6845 ± 30				
id.	**15**	Organic layer	GIF10635	QLB4	−14.9	7320 ± 80	(0.96)7937–8215/ 8076 ± 139			
id.	**15.1**	Marine shell	GIF11450	QLB20	−0.9	7310 ± 50				
id.	**16**	Organic layer	GIF10636	QLB5	−16.3	6940 ± 60	(1.00) 7592–7849/ 7721 ± 129			
id.	**16.1**	Marine shell	GIF11451	QLB21	0.0	7095 ± 50				
id.	**17**	Charcoal	GIFA97287	B3NIV2A	−15.6	6460 ± 60	(0.96) 7242–7432/ 7337 ± 95			
id.		*Charcoal*	*GIFA97288*	*C1NIV2A*	*−22.0*	*6510 ± 60*				
id.	**17.1**	Marine shell	GIF10399	N2a	−3.0	6110 ± 80				
Caserones: 19°55'S, 69°31'W										
Southon et al. (1995)		*Yarn*	*CAMS9372*	*CAS512*	*−20*	*1630 ± 70*				
id.	**1**	Yarn	CAMS9373	CAS512	−20	1560 ± 50	(0.77) 1307–1449/ 1378 ± 71	**1779 ± 26 1905 ± 26**		
id.	**1.1**	**Feather**	**CAMS7610**	**CAS512**	**-13.4**	**2120 ± 90**			**278 ± 66**	**-92.6 ± 18.0**
id.	**1.2**	**Feather**	**CAMS9374**	**CAS512**	**-13.4**	**2040 ± 50**			**198 ± 40**	**-83.5 ± 13.6**
id.	**2**	Yarn	CAMS10314	CASTr6/7	−20.2	1690 ± 60	(0.91) 1392–1637/ 1515 ± 123	**1860 ± 26 2069 ± 27**		
id.	**2.1**	**Feather**	**CAMS10315**	**CASTr6/7**	**-11.5**	**2170 ± 60**			**206 ± 46**	**-83.2 ± 20.4**
id.	**2.2**	**Bird skin**	**CAMS10316**	**CASTr6/7**	**-12.2**	**2280 ± 50**			**316 ± 40**	**-95.6 ± 19.0**
id.	**3**	Yarn	CAMS10317	CAS93.031	−20.4	1850 ± 70	(1.00) 1550–1876/ 1713 ± 163	**2001 ± 27 2271 ± 26**		
id.	**3.1**	**Feather**	**CAMS10318**	**CAS93.031**	**-13.1**	**2310 ± 100**			**174 ± 73**	**-77.2 ± 29.7**
id.	**3.2**	**Bird skin**	**CAMS10319**	**CAS93.031**	**-13.6**	**2290 ± 60**			**154 ± 46**	**-74.9 ± 25.2**
id.	**4**	Plant fiber	CAMS10320	CAS572	−23.5	1270 ± 60	(0.91) 1049–1278/ 1164 ± 115	**1503 ± 26 1730 ± 26**		
id.	**4.1**	**Fish vertebra**	**CAMS10321**	**CAS572**	**-12.8**	**1740 ± 50**			**124 ± 40**	**-73.0 ± 18.6**
id.	**4.2**	**Skin? stomach?**	**CAMS10322**	**CAS572**	**-14.5**	**1800 ± 60**			**184 ± 46**	**-79.9 ± 19.6**
Pta.Guanillo: 21°58'S, 70°11'W										
This work	**1**	Charcoal	Pa 1909	C00-406	−25.8	2865 ± 140	(0,99) 2702–3360/ 3031 ± 329			
id.	**1.1**	*C. concholepas*	Pa 1931	C00-411	−0.5	2930 ± 70				
id.	**1.2**	*Fissurellasp.*	Pa 1932	C00-407	0.9	3100 ± 40				
id.	**2**	Yarn	Pa 2264			630 ± 40	(0.60) 581–650/ 616 ± 35			
id.	**2.1**	*Protothaca thaca*	Pa 2265		–	1027 ± 40				
La Chimba: 13: 23°34'S, 70°22'W										
This work	**1**	Charcoal	TO-6526	N23/W07	–	9460 ± 90	(0.88)10372–10876/ 10624 ± 252			
id.	**1.1**	Marine shell	UQ-2156	N23/W07	–	9088 ± 120				
id.	**2**	Charcoal	TO-6528	N23/W07	–	9910 ± 90	(0.98)10090–11645/ 11368 ± 278			
id.	**2.1**	Marine shell	UQ-2157	N23/W07	–	9163 ± 140				
id.	**3**	Charcoal	TO-6527	N02/W14	–	9260 ± 90	(1.00)10205–10587/ 10396 ± 191	**9367 ± 27 9762 ± 30**		
id.	**3.1**	**Marine shell**	**TO-6320**	**N02/W14**	**–**	**9800 ± 80**			**236 ± 60**	**38.4 ± 34.3**

several valves of bivalves) which should thus provide representative interannual values of their radiocarbon content and should integrate intrashell seasonal variability (Culleton et al., 2006; Jones et al., 2007). Most analyzed shells correspond to animals that commonly live several years, which implies that there are not susceptible to record short-lived oceanographic phenomena, like El Niño events which only

last a few months, at most. The shell samples, which did not show any evidence for recrystallisation, were submitted to preliminary surficial cleaning (ultrasonic bath with 1 M HCl). Charcoal fragments were prepared using standard treatments (Acid-Alkali-Acid). The isotopic ratios were measured by LSC on a mass spectrometer Isogas (Optima) and the radiocarbon activity determined by beta counting on a Packard TRI-CARB 2260 XL.

All the radiocarbon results, from marine and terrestrial samples, are expressed as conventional ages, after normalization of $\delta^{13}C = -25‰$ (Stuiver and Polach, 1977). The terrestrial ages were calibrated using the Calib5.0.1 software and the method of probabilities (Stuiver and Reimer, 1993; Stuiver et al., 1998) for Southern Hemisphere terrestrial samples (McCormac et al., 2002, 2004), taking the two-sigma calibrated age range (95.4% of probabilities).

ΔR and $\Delta^{14}C_t$ calculations

For the Δ*R* estimates of each pair of samples, following Southon et al. (1995), we used a direct approach calculating the differences between the measured marine radiocarbon data and the corresponding age from the marine calibration curve (Hughen et al., 2004). For each two-sigma terrestrial calibrated age range, the marine calibration curve provided maximum and minimum radiocarbon values. We calculated a minimum and a maximum Δ*R* as the difference between the measured conventional marine age and those values. Finally, we have taken the arithmetic mean as the most representative Δ*R* value corresponding to this one-sigma terrestrial calibrated age range. Calculations are summarized as follow:

$$\Delta R_{min} = Age_{marine\ sample} - Age_{marine\ curve\ maximum}$$
$$\Delta R_{max} = Age_{marine\ sample} - Age_{marine\ curve\ minimum}$$
$$\Delta R = (\Delta R_{min} + \Delta R_{max})^{*}0.5$$

Errors were propagated according to the formula:

$$\sigma_R = \left(\sigma^2_{marine\ sample} + \sigma^2_{marine\ curve}\right)^{1/2}$$

The marine $\Delta^{14}C_t$ values were calculated from the difference between the measured marine radiocarbon age, based on the Cambridge half-life, and the mean value of the corresponding terrestrial calibrated age range, applying the formula of Stuiver and Polach (1977):

$$xc - t' = 8267^{*}\ln\left(1 + \Delta^{14}C_t / 1000\right),$$

where t' is the radiocarbon age calculated with the Cambrige half-life (5730 yr) and xc is the mean calibrated age range (cal yr BP). $\Delta^{14}C_t$ errors were calculated from the maximum and minimum differences associated to the measurements and their respective uncertainties.

Regional reservoir-effect estimates

Calendar vs. marine conventional age comparison

In this study, 19 localities were considered, six from previous work by other authors and 13 sampled by us (Figs. 2 and 3). In some localities, different chronostratigraphic units were sampled. The number of pairs, including the cases in which the results of more than one marine sample are compared to the result of a single terrestrial sample, amounts to 73.

Results of radiocarbon measurements of all the studied pairs (Table 1) are shown in Figure 4. Pairs yielding positive values of Δ*R* (46) are indicated as crosses above the marine calibration curve of Figure 4, while the values located below it (27) correspond to pairs with either a negative Δ*R*, or for which the terrestrial material was significantly older than the corresponding marine sample ("old wood" samples). It could be argued that Δ*R* values falling below the marine calibration curve of Figure 4 might be significant. We do not think so, because we consider as quite improbable a perceptible effect of former incursions of equatorial waters, with high $\Delta^{14}C$ values, on the isotopic composition of the marine shells. Even if southward invasions of equatorial waters occurred in the past, for instance during strong ENSO events, the duration of the phenomenon (a few months at most) would have been too short to impact on the global content of ^{14}C of the whole analysed shells. Therefore, we interpret that none of the Δ*R* values which are figured below the marine calibration curve actually reflect reliable data. This means that we cannot use the data corresponding to these 27 pairs of marine/terrestrial samples.

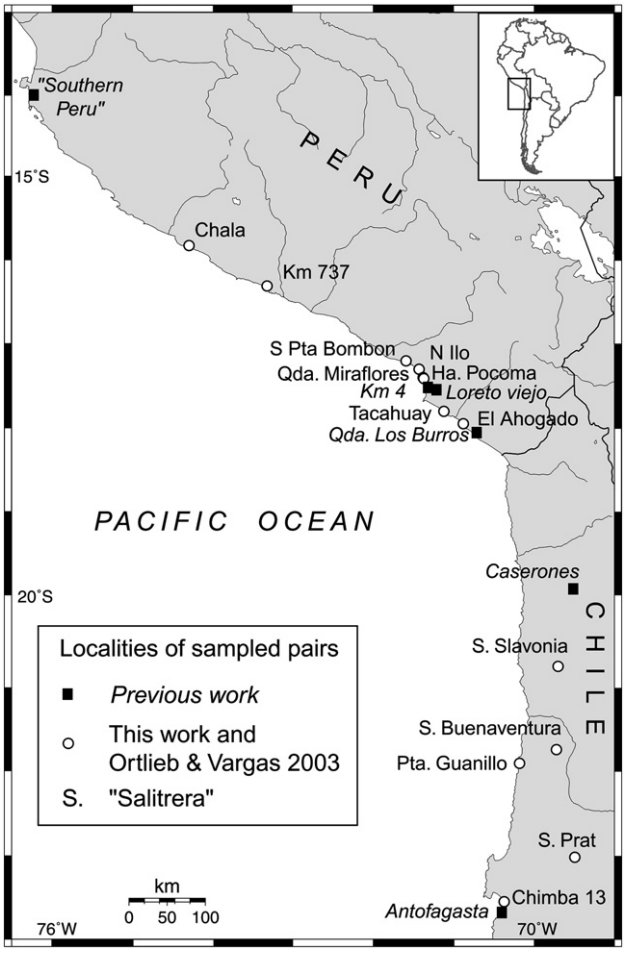

Figure 2. Sketch map with localities mentioned in the paper. Italics refer to sampling localities of previous authors (Taylor and Berger, 1967; Southon et al., 1995; Owen, 2002; Kennett et al., 2002; Fontugne et al., 2004; see Table 1). See also Ortlieb and Vargas, 2003.

The study thus confirms previous observations and inferences made in the study area (Southon et al., 1995; Kennett et al., 2002; Owen, 2002; Fontugne et al., 2004) which emphasized the difficulty in obtaining reliable estimates of the radiocarbon age of archaeological samples. However, our compilation and treatment of previous and new radiocarbon data on pairs of associated material in the study area leads us to pinpoint 46 pairs of marine-terrestrial radiocarbon data which provide positive estimates of Δ*R* values at different periods during the Holocene. Considering that these pairs, which represent more than half of the compiled new and previous data (Table 1), are rather well distributed geographically within the study area (Fig. 2), we assume that these results constitute a statistically significant set of data to evaluate major changes of Δ*R* and its variability at different time periods during the Holocene.

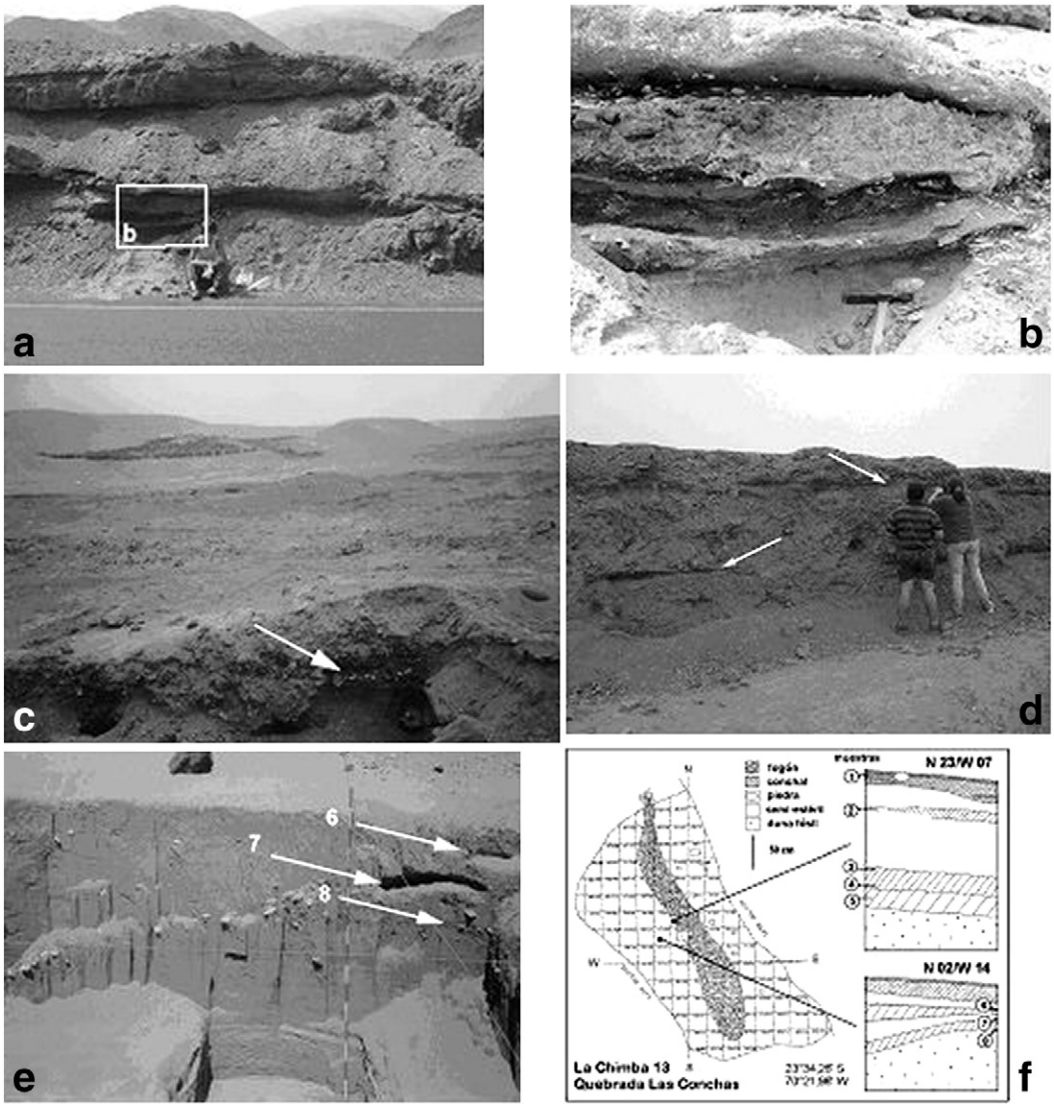

Figure 3. Illustration of some of the sampling sites (see Fig. 2 for location and Table 1 for analytical results). a and b: Km 737 of the Pan-American Highway locality; a: Left: roadcut showing the superposition of debris-flow units separated by sandy layers; b: detail view of kitchen midden remains associating marine shells (mostly *Mesodesma donacium)* and charcoals or ashy lenses. The two upper fossiliferous unconsolidated sandy layers, at right, provided the samples P03–48/49 (top) and P03–45/46/47 (center of the photo) (see Table 1). c: Hacienda Pocoma archaeological deposit with human burials. Associated shells (P01–28/30) and charcoal (P01–27) and plant remains (P01–29) were radiocarbon dated. d: Quebrada Miraflores locality: studied samples are marine shell remains (P03–51) and associated charcoals fragments (P03–50) interstratified between debris flow units. e and f: Location of sampled pairs in the archaeological site of Chimba 13, Antofagasta. e: excavation N02/W14, showing the hole (upper right, "6") where samples 6a/b (Table 1) were taken. f: general map and schematic sections of the two excavations of the site.

Variability of ΔR during the Holocene

The new data set presented here which provides a series of positive ΔR estimates (10th column in Table 1) covers, although unequally, the whole Holocene Period. Variations of those values during the Holocene, as well as the total range of variability for a specific period, are shown in Figure 5. These results lead to distinguish three periods, the early Holocene, the middle Holocene and the last millennium.

A high variability is observed during the early Holocene, from $10{,}396 \pm 191$ until 6844 ± 179 cal yr BP, with maximum values of $\Delta R = 1057 \pm 47$ yr). A mean ΔR value of 511 ± 278 yr is calculated for this period of the early Holocene. Following this period, the ΔR drops dramatically both in mean value and total range of variability. Actually, between 5184 ± 149 and 1164 ± 115 cal yr BP, the marine reservoir effect shows much less variability, with maximum values of $\Delta R = 344 \pm 46$ yr, and a mean ΔR value of 226 ± 98 yr. Between 638 ± 84 and 396 ± 78 cal yr BP, our results suggest an increase in variability of the regional marine reservoir effect, with maximum values of $\Delta R = 499 \pm 33$ yr, with a mean ΔR value of 355 ± 105 yr. This tendency is confirmed by the regional marine reservoir effect estimated from the mollusc shells collected in the *salitreras*, period comprised between 41 ± 9 and 15 ± 5 cal yr BP, with maximum values of $\Delta R = 670 \pm 35$ yr, and a mean ΔR value of 253 ± 207 yr.

Previous studies in the region (Southon et al., 1995; Owen, 2002; Kennett et al., 2002; Fontugne et al., 2004) discussed the pervasiveness of the original ΔR value determined by Taylor and Berger (1967). Our results suggest that both the variability and the mean value of ΔR have been much higher even during the modern pre-bomb period (first half of the 20th century) than initially suggested by these authors, who actually based their calculations on a quite limited number of marine shells. The new radiocarbon measurements obtained from mollusc shells collected in the *salitreras* provide a more reliable set of data for the estimation of the modern pre-bomb mean value of the ΔR and its range of variability.

The data set shows an increase of ΔR value since 638 cal yr BP, with respect to the previous period in the middle Holocene. This increase is depicted by pairs of samples which provided the highest values of ΔR

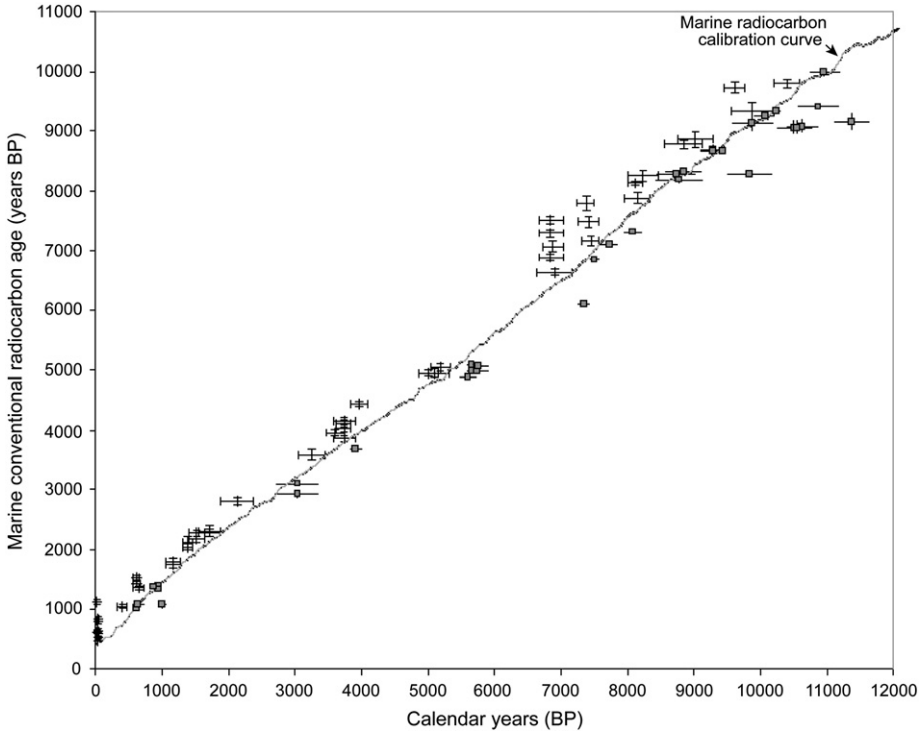

Figure 4. Calendar vs. marine conventional radiocarbon ages obtained in the study area (see Table 1). Crosses indicate positive values of Δ*R*, which are used in further calculations, while filled squares pinpoint negative Δ*R* values (revealing "old wood" effect and similar unreliable cases) that are discarded for the calculations (see Fig. 4). Error bars correspond to 2σ ranges. The calibration curve for Southern Hemisphere terrestrial samples is according McCormac et al. (2002, 2004).

(Fig. 5), but is supported by the mean values of Δ*R* and their associated standard deviations. Thus, our observations confirm that previous interpretations which had considered a constant Δ*R* value during the middle to late Holocene (Southon et al., 1995; Fontugne et al., 2004) should be revised.

Beside some high Δ*R* values around 3740–3970 cal yr BP, and the lack of data between two one-thousand-year periods (3250–2130 cal yr BP and 5010–3970 cal yr BP), the lower mean value and total range of variability of Δ*R* seem to be well constrained for the middle early-late Holocene period between 5180 and 1160 cal yr BP.

The lack of data between 6840 and 5180 cal yr BP impedes a more precise chronological determination for the major change in both the mean value and the total range of variability of Δ*R* at that time. However, the magnitude of this change suggests an abrupt decrease of Δ*R* from an early Holocene stage to a middle Holocene stage, in a short time interval (about 1660 yr), after 6840 cal yr BP. In this sense, our results provide more precise information than the previous work of Fontugne et al. (2004), which assumed high values of Δ*R* until about 4000 cal yr BP.

Δ*R*, upwelling and major oceanographic changes during the holocene

Variation throughout the Holocene of Δ*R* values may reflect combinations of effects from varying upwelling intensity and changes in the circulation of water masses. The high Δ*R* values (i.e. low $\Delta^{14}C_t$) that characterized the early Holocene until ca. 6840 cal yr BP strongly decreased from ca. 5180 cal yr BP onward (Fig. 6). The dramatic change in both the maximum values of Δ*R* and the Δ*R* range of variability observed during this lapse suggests a major oceanographic change in the Humboldt Current system before the mid Holocene which seems to be supported by some paleoceanographic data along the Chilean margin and in the southern ocean.

From alkenone analyses in sediment core GIK17748-2 located at 33°S, Kim et al. (2002) inferred an important increase in SST conditions ca. 7800 cal yr BP, after cooler sea surface conditions during the early Holocene, followed by a slight decrease in SST values during the second half of the Holocene. According to Kim et al. (2002), low SST conditions during the early Holocene resulted probably from a northward location of the west-drifted Antarctic Circumpolar Current (ACC), which was located closer to the pole during the mid Holocene and afterward. Additionally, paleoclimatic and paleoceanographic data from and off north-central Chile suggest that the early Holocene was characterized by an increased aridity, most probably related to a strengthened SEPSA (Heusser, 1990; Villagrán and Varela, 1990; Veit, 1996; Grosjean et al., 1997; Lamy et al., 1998, 1999, 2000; Jenny et al., 2002, 2003; Villa-Martínez et al., 2003; Vargas et al., 2006), with associated intensified coastal upwelling and decreased coastal SSTs (Vargas et al., 2006). We contend that a strengthened SEPSA and a northward location of the ACC favored the shoaling of ^{14}C-depleted water masses, through increased influence of equatorial subsurface waters (ESSW) in strengthened coastal upwelling processes in the study area, together with an intensified northward advection of subantarctic waters and probably some intermediate waters, as the eastern south Pacific intermediate water (ESPIW) which is formed in the south-eastern limb of the SEPSA and advected northward along the central Chilean margin (Schneider et al., 2003). If this interpretation is correct, high Δ*R* values should also have characterized the surface water masses off subtropical central Chile. Considering this last hypothesis, we recalibrated the radiocarbon ages of the core GIK17748-2 (Kim et al., 2002) using our Δ*R* estimates for the northern Chile-southern Peru region and recalculated the chronological model for this core. The consistency between the Holocene evolution of the marine $\Delta^{14}C_t$ estimated from our compiled dataset in the study region and the recalibrated chronology for the inferred SST values off central Chile (Fig. 6) supports the idea that a drastic diminution of the Δ*R* values occurred shortly ca. 6840 cal yr BP, as the result of a change in oceanographic conditions in the Peru-Chile Current after ca. 7150 cal yr BP. Additionally, the higher marine radiocarbon reservoir effect estimated for the early Holocene with respect to the mid and late Holocene in the southern ocean (van Beek et al., 2002), suggests that the last change resulted from a major reorganization in oceanographic circulation within the subantarctic region. In fact, a strong

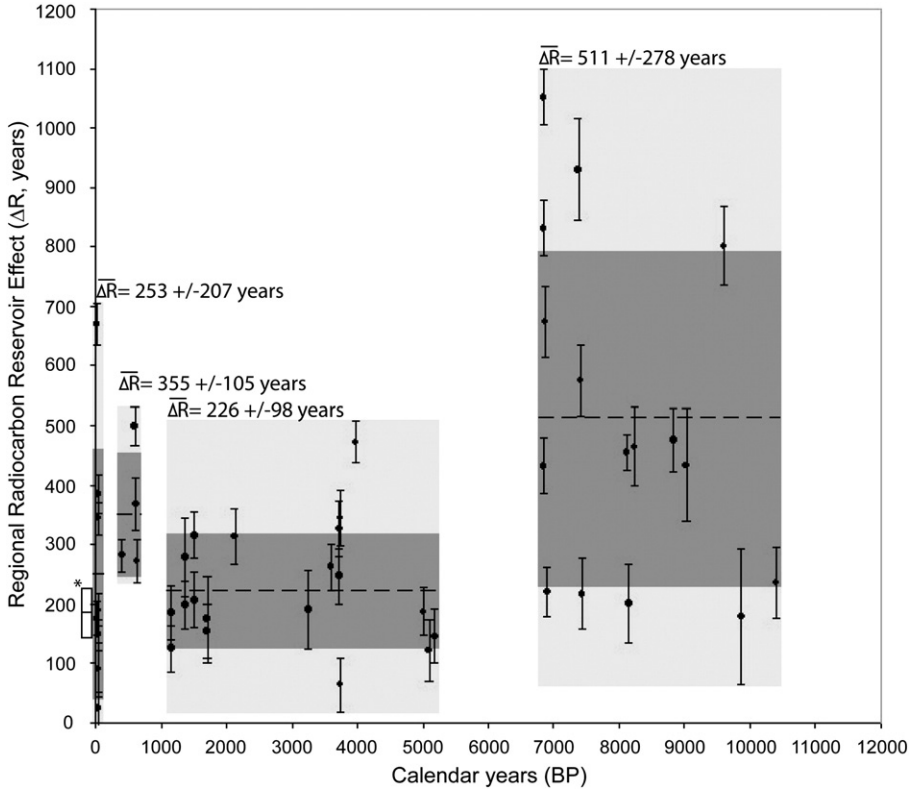

Figure 5. Compilation of regional reservoir effect (ΔR) values throughout Holocene times, expressed in years, calculated on validated samples (10th column in Table 1) from the southern Peru-northern Chile region (see Fig. 4). Error bars correspond to 2σ ranges. Mean and associated 2σ values calculated for each period in this work are also indicated (dark and light grey areas, respectively). The asterisk (*) indicates the $\Delta R = 190 \pm 40$ yr value (Taylor and Berger, 1967; Stuiver and Braziunas, 1993) commonly used in the region by most authors.

argument for a drastic change in the regional circulation pattern at that time is provided by a sediment core extracted in the Ross Sea, in Antarctica, which indicates a rapid landward recession of the Antarctic glaciers together with the onset of seasonal sea-ice formation between 8000 and 7800 BP (Finocchiaro et al., 2005). The time-lag between changes in Antarctica and the Peru-Chile Current domain may be explained by the important reservoir effect during the early Holocene in the subantarctic region (van Beek et al., 2002). If the current general circulation system of the Ross Sea and the formation of high-salinity shelf water (HSSW) in the Antarctic Ocean were actually set at 7.8 ka, it can be inferred that drastic changes also occurred at that time in the Peru-Chile Current system, through remote mechanism (Toggweiler et al., 1991) or directly on the ^{14}C-content of the subantarctic waters.

Multiproxy analyses from a marine core located at 41°S, where the AAC is deflected toward the north, suggested a significant increase of productivity and a SST cooling (by as much as 1.4 °C) during the last 1500 yr of the record (Lamy et al., 2002), consistently with a similar tendency in the SST values observed off central Chile (Kim et al., 2002; Fig. 6). This recent evolution within the southern part of the Peru-Chile Current system has been attributed to an equatorward shift of the AAC and of the westerlies (Kim et al., 2002; Lamy et al., 2002). This oceanographic change should be contemporaneous with the increase of mean ΔR values that is observed in the last ~7 centuries, within the study area, which could be associated to a higher influence of ESSW in the upwelled waters, through increased climatic forcing due to southerly coastal winds in the eastern rim of the subtropical anticyclone. In fact, the high variability of the ΔR values, particularly during the early twentieth century but also between 638 ± 84 and 396 ± 78 cal yr BP, may reflect a higher variability of both, upwelling and subtropical water masses related to ENSO, contemporaneously with a higher frequency of ENSO-related climate anomalies inferred from the study of debris flow sequences during the last thousand years with respect to the earlier part of the late Holocene (Vargas et al., 2006).

Conclusions

Variations of radiocarbon regional reservoir effect reflect paleoceanographic changes in the composition and circulation pattern of subsuperficial waters, as well as variations in the intensity of upwelling phenomena. Tropical coastal regions like that of southern Peru and northern Chile, submitted to strong upwelling processes, commonly experience high values of ΔR and are prone to variations of these ΔR values through time, according to paleoceanographic regime changes.

This study provides a new set of data which allowed us to estimate mean ΔR values and the variability range of these values throughout the Holocene along the 14°–24°S coastal area of western South-America. The compilation of previous data and of a new series of associated pairs of marine shells and charcoal fragments, led us to sort out the numerous cases in which the "old wood" effect prevent any calculation of ΔR values from radiocarbon measurements in the marine carbonates. The practical result of the study is a reconstruction of ΔR values in 46 pairs of associated marine/atmospheric material widely distributed in the whole study area, and which cover almost all the Holocene period.

It is thus shown that the extrapolation of modern ΔR values, which had been determined on a limited number of pre-bomb modern shells (Taylor and Berger, 1967), cannot be justified, even for the past few thousand years (Southon et al., 1995; Fontugne et al., 2004).

In terms of paleoceanographic implications, our results confirm that old ^{14}C-depleted water masses found in the study area come from the Antarctic and subantarctic region and that variation of their ΔR values during the early to mid Holocene were associated to the ACC and the Peru-Chile Current dynamics. Part of these changes could be tentatively linked to variations in the advection regime of old waters that reach the study area through a thermohaline mechanism as proposed by Toggweiler et al. (1991). Very high ΔR values occurred during the early Holocene and particularly around 7500–7000 cal yr BP, in close

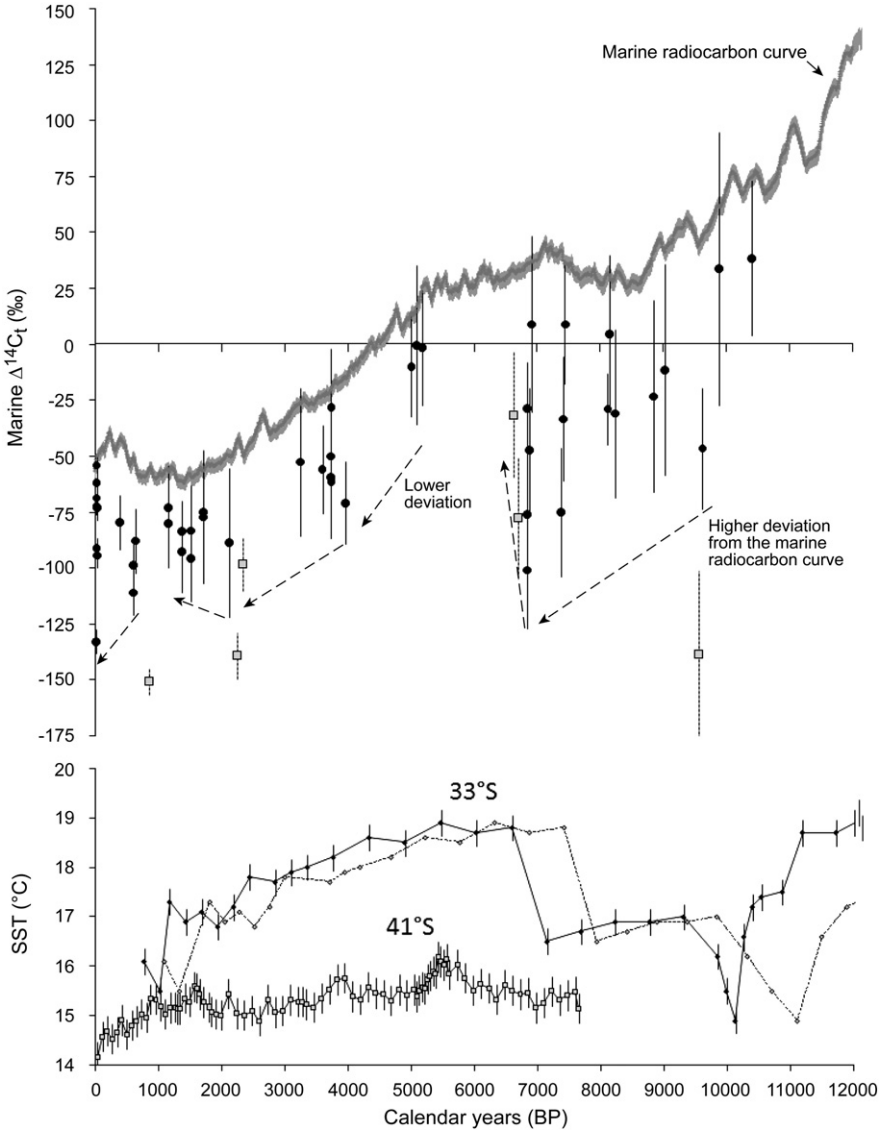

Figure 6. Top: marine $\Delta^{14}C_t$ values (‰) calculated from the mean marine radiocarbon age range and the corresponding calibrated terrestrial pair of radiocarbon data in the southern Peru-northern Chile region (black circles), plotted with respect to the $\Delta^{14}C_t$ values of the marine calibration curve (Hughen et al., 2004). Grey squares show marine $\Delta^{14}C_t$ values estimated from sediment records in the Antarctic region (Van Beek et al., 2002). The variation of the negative deviation of the data from northern Chile-southern Peru and Antarctic regions, with respect to the calibration curve, represents the magnitude of the regional radiocarbon reservoir effect throughout the Holocene in specific moments, in both areas. Arrows indicate the tendencies of the maximum deviations of the marine $\Delta^{14}C_t$ values estimated in this work, with respect to the $\Delta^{14}C_t$ values in the global marine calibration curve (Hughen et al., 2004). Bottom: Alkenone-based SST reconstructions from sediment cores at 33°S (Kim et al., 2002; doted line) according a revised chronological model extrapolated from new ΔR estimates in northern Chile and southern Peru (solid line; this work) and 41°S (Kim et al., 2002).

relationship with a profound re-accommodation of oceanographic circulation patterns in the southern ocean which affected the Peru-Chile Current. The ΔR values diminished significantly probably shortly after 6840 cal yr BP, in any case before 5180 cal yr BP, and not as late as 4000 cal yr BP, as suggested previously (Fontugne et al., 2004).

Impacts of ENSO-related climate anomalies in the area seem to have been set up only after about 5300–5500 cal yr BP (Vargas et al., 2006), and after the pre-mid-Holocene reorganization of the southeast Pacific and circum-Antarctic circulation patterns. During the mid-Holocene, the higher SST values off central Chile and the increased influence of ENSO in the region probably favored the inclusion of subtropical waters in the surface circulation of the study region and southward migration of the oceanographic front related to the ESPIW, presently located at 32ºS, reducing also the contribution of ESSW in the upwelling events. The higher values and range of variability of ΔR values observed in the last seven centuries reflect an increased influence of ^{14}C-depleted water masses in the upwelling events, contemporaneously with increased ENSO variability in the region as suggested by other proxies in the area.

Acknowledgments

The study was mainly supported by IRD projects (PVC in 1997–2000, PALEOTROPIQUE in 2001–2008) in the framework of scientific agreements with the Universidad de Chile, Instituto Geofísico del Perú and Universidad de Antofagasta. Preparation of most of the samples for radiocarbon measurements, and part of the classical ^{14}C dating were performed in the LOCEAN (formerly LODYC) laboratory (CNRS-Univ. Paris 6-IRD-MNHN).

Some radiocarbon analyses (Chimba 13, Antofagasta) were obtained through FONDECYT Project #1950036 (PI: A. Llagostera). Field work, which began in 1990, involved J. Macharé (Instituto Geofísico del Perú), N. Guzman (IRD), M. Soto (IRD) and other collaborators and students from Chile and Peru: their assistance was greatly appreciated. Thanks are also due to M. Mandeng Yogo (IRD) who prepared some of the samples and realised some of the stable isotope and radiocarbon analyses.

The authors are grateful to the three reviewers who helped to improve significantly the manuscript.

References

Albero, M.C., Angiolini, F.E., Piana, E.L., 1986. Discordant ages related to reservoir effect of associated archaeologic remains from the Tunnel site, Beagle Channel, Argentine Republic. Radiocarbon 28, 748–753.

Angulo, R.J., Reimer, P.O.J., de Souza, M.C., Scheel-Ybert, R., Tenório, M.C., Disaró, S.T., Gaspar, M.D., 2007. A tentative determination of upwelling influence on the paleosurficial marine water reservoir effect in Southeasten Brasil. Radiocarbon 49, 1255–1259.

Bard, E., Arnold, M., Mangerud, J., Paterne, M., Labeyrie, L., Duprat, J., Melieres, M.A., Sonstegaard, E., Duplessy, J.C., 1994. The North Atlantic atmosphere–sea surface ^{14}C gradient during the Younger Dryas climatic event. Earth and Planetary Science Letters 126, 275–287.

Brandhorst, W., 1971. Condiciones oceanográficas estivales frente a la costa de Chile. Revista de Biología Marina (Valparaiso) 14 (3), 45–84.

Broecker, W.S., Andree, M., Bonani, G., Wolfli, W., Oeschger, H., Klas, M., Mix, A., Curry, W., 1988. Preliminary estimates for the radiocarbon age of deep water in the glacial ocean. Paleoceanography 3, 659–669.

Burr, G.S., Beck, J.W., Corrège, T., Cabioch, G., Taylor, F.W., Donahue, D.J., 2009. Modern and Pleistocene reservoir ages inferred from South Pacific corals. Radiocarbon 51, 319–335.

Culleton, B.J., Kennett, D.J., Ingram, B.L., Erlandson1, J.M., Southon, J.R., 2006. Intrashell radiocarbon variability in marine molluscs. Radiocarbon 48, 387–400.

Dezileau, L., Ulloa, O., Hebbeln, D., Lamy, F., Reyss, J.L., Fontugne, M., 2004. Iron control of past productivity in the coastal upwelling system off the Atacama Desert, Chile. Paleoceanography 19, PA3012 doi:10.1029/2004PA001006.

Dye, T., 1994. Apparent ages of marine shells: implications for archaeological dating in Hawai'i. Radiocarbon 36, 51–57.

Eiriksson, J., Larsen, G., Knudsen, K.L., Heinemeier, J., Simonarson, L.A., 2004. Marine reservoir age variability and water mass distribution in the Iceland Sea. Quaternary Science Reviews 23, 2247–2268.

Fallon, S.J., Guilderson, T.P., 2008. Surface water processes in the Indonesian throughflow as documented by a high-resolution coral Δ14C record. Journal of Geophysical Research 113, C09001 doi:10.1029/2008JC004722.

Finocchiaro, F., Langone, L., Colizza, E., Fontolan, G., Giglio, F., Tuzzi, E., 2005. Record of the early Holocene warming in a laminated sediment core from Cape Hallett Bay (Northern Victoria Land, Antarctica). Global and Planetary Change 45, 193–206.

Fontugne, M., Carré, M., Bentaleb, I., Julien, M., Lavallée, D., 2004. Radiocarbon reservoir age variations in the south Peruvian upwelling during the Holocene. Radiocarbon 46, 531–537.

Goslar, T., Arnold, M., Bard, E., Kuc, T., Pazdur, M., Ralska-Jasiewiczowa, M., Roanski, K., Tinserat, N., Walanus, A., Wicik, B., Wieckowski, K., 1995. High concentrations of atmospheric ^{14}C during the Younger Dryas cold episode. Nature 377, 414–417.

Grosjean, M., Valero-Garcés, B., Geyh, B., Messerli, M.A., Schotterer, U., Schreier, H., Kelts, K., 1997. Mid- and late-Holocene limnogeology of Laguna del Negro Francisco, northern Chile, and its palaeoclimatic implications. Holocene 7, 151–159.

Head, J., Jones, R., Allen, J., 1983. Calculation of the marine reservoir effect from the dating of shell-charcoal paired samples from an aboriginal midden on Great Glennie Island, Bass Strait. Australian Archaeology 17, 99–112.

Hebbeln, D., Marchant, M., Freudenthal, T., Wefer, G., 2000. Surface distribution along the Chilean continental slope related to upwelling and productivity. Marine Geology 164, 119–137.

Hebbeln, D., Marchant, M., Wefer, G., 2002. Paleoproductivity in the southern Peru–Chile Current through the last 33, 000 yr. Marine Geology 186, 487–504.

Heusser, C.J., 1990. Ice age vegetation and climate of subtropical Chile. Palaeogeography, Palaeoclimatology, Palaeoecology 80, 107–127.

Hughen, K.A., Overpeck, J.T., Lehman, S.J., Kashgarian, M., Southon, J., Peterson, L.C., Alley, R., Sieman, D.M., 1998. Deglacial changes in ocean circulation from an extended radiocarbon calibration. Nature 391, 65–68.

Hughen, K.A., Baillie, M.G.L., Bard, E., Beck, J.W., Bertrand, C.J.H., Blackwell, P.G., Buck, C. E., Burr, G.S., Cutler, K.B., Damon, P.E., Edwards, R.L., Fairbanks, R.G., Friedrich, M., Guilderson, T.P., Kromer, B., McCormac, G., Manning, S., Ramsey, C.B., Reimer, P.J., Reimer, R.W., Remmele, S., Southon, J.R., Stuiver, M., Talamo, S., Taylor, F.W., van der Plicht, J., Weyhenmeyer, C.E., 2004. Marine04 marine radiocarbon age calibration, 0-26 cal kyr BP. Radiocarbon 46, 1059–1086.

Ingram, B., 1998. Differences in radiocarbon age between shell and charcoal from a Holocene shellmound in northern California. Quaternary Research 49, 102–110.

Jenny, B., Valero-Garcés, B.L., Villa-Martínez, R., Urrutia, R., Geyh, M.A., Veit, H., 2002. Early to mid-Holocene Aridity in Central Chile and the Southern Westerlies: The Laguna Aculeo Record (34ºS). Quaternary Research 58, 160–170 doi:10.1006/qres.2002.2370.

Jenny, B., Willhelm, D., Valero-Garcés, B., 2003. The southern westerlies in Central Chile: Holocene precipitation estimates based on a water balance model for Laguna Aculeo (33º50' S). Climate Dynamics 20, 269–280.

Jones, K.B., Hodgins, G.W.L., Dettman, D.L., Andrus, C.F.T., Nelson, A., Etayo-Cadavid, M. F., 2007. Seasonal variations in Peruvian marine reservoir age from prebomb *Argopecten purpuratus* shell carbonate. Radiocarbon 49, 877–888.

Kennett, D.J., Ingram, B.L., Erlandson, J.M., Walker, P., 1997. Evidence for temporal fluctuations in marine radiocarbon reservoir ages in the Santa Barbara Channel, Southern California. Journal of Archaeological Science 34, 1051–1059.

Kennett, D.J., Ingram, B.L., Southon, J., Wise, K., 2002. Differences in ^{14}C age between stratigraphically associated charcoal and marine shell from archaic period site of kilometer 4, southern Peru: old wood or old water? Radiocarbon 44, 53–58.

Kim, J.-H., Schneider, R., Hebbeln, D., Müller, P.J., Wefer, G., 2002. Last deglacial sea-surface temperature evolution in the Southeast Pacific compared to climate changes on the South American continent. Quaternary Science Reviews 21, 2085–2097.

Kovanen, D.J., Easterbrook, D.J., 2002. Paleodeviations of radiocarbon marine reservoir values for the northeast Pacific. Geology 30, 243–246.

Kwiecien, O., Arz, H.W., Lamy, F., Wulf, S., Bahr, A., Röhl, U., Haug, G.H., 2008. Estimated reservoir ages of the black sea since the last Glacial. Radiocarbon 50, 99–108.

Lamy, F., Hebbeln, D., Wefer, G., 1998. Late Quaternary processional cycles of terrigenous sediment input off the Norte Chico, Chile (27.58 S) and paleoclimatic implications. Palaeogeography, Palaeoclimatology, Palaeoecology 141, 233–251.

Lamy, F., Hebbeln, D., Wefer, G., 1999. High-resolution marine record of climatic change in mid-latitude Chile during the last 28, 000 years based on terrigenous sediments parameters. Quaternary Research 51, 83–93.

Lamy, F., Klump, J., Hebbeln, D., Wefer, G., 2000. Late Quaternary rapid climate change in northern Chile. Terra Nova 12, 8–13.

Lamy, F., Rühlemann, C., Hebbeln, D., Wefer, G., 2002. High- and low-latitude climate control on the position of the southern Peru-Chile Current during the Holocene. Paleoceanography 17, 1028 doi:10.1029/2001PA000727.

Lamy, F., Kaiser, J., Ninnemann, U., Hebbeln, D., Arz, H.W., Stoner, J., 2004. Antarctic Timing of Surface Water Changes off Chile and Patagonian Ice Sheet Response. Science 304, 1959–1962.

Lewis, C.A., Reimer, P.J., Reimer, R.W., 2008. Marine reservoir corrections; St. Helena, South Atlantic Ocean. Radiocarbon 2008 (50), 275–280.

Little, E., 1993. Radiocarbon age calibration at the archaeological sites of coastal Massachusetts and vicinity. Journal of Archaeological Science 20, 457–471.

Marchant, M., Hebbeln, D., Wefer, G., 1999. High resolution record of the last 13, 300 years from the upwelling area off Chile. Marine Geology 161, 115–128.

McCormac, F.G., Reimer, P.J., Hogg, A.G., Higham, T.F.G., Baillie, M.G.L., Palmer, J., Stuiver, M., 2002. Calibration of the radiocarbon time scale for the southern hemisphere: AD 1850-950. Radiocarbon 44, 641–651.

McCormac, F.G., Hogg, A.G., Blackwell, P.G., Buck, C.E., Higham, T.F.G., Reimer, P.J., 2004. SHCal04 Southern Hemisphere calibration, 0-11.0 cal kyr BP. Radiocarbon 46, 1087–1092.

Morales, C.E., Blanco, J.L., Braun, M., Reyes, H., Silva, N., 1996. Chlorophyll-a distribution and associated oceanographic conditions off northern Chile during the winter and spring 1993. Deep-Sea Research 43, 267–389.

Muscheler, R., Beer, J., Wagner, G., Finkel, R.C., 2000. Changes in deep-water formation during the Younger Dryas event inferred from ^{10}Be and ^{14}C records. Nature 408, 567–570.

Ndeye, M., 2008. Marine Reservoir ages in northern Senegal and Mauritania coastal waters. Radiocarbon 50, 281–288.

Ortlieb, L., Vargas, G., 2003. Debris-flow deposits and El Niño manifestations along the hyperarid southern Peru/northern Chile coast. In: Haas, J., Dillon, M.O. (Eds.), El Niño in Peru: Biology and culture over 10,000 years: Fieldiana Botany, vol. 34, pp. 24–51.

Owen, B.D., 2002. Marine reservoir age estimates for the far south coast of Peru. Radiocarbon 44, 701–708.

Petchey, F., Anderson, A., Zondervan, A., Ulm, S., Hogg, A., 2008. New marine Δ*R* values for the South Pacific Subtropical Gyre. Radiocarbon 50, 373–397.

Phelan, M., 1999. A Δ*R* correction value for Samoa from known-age marine shells. Radiocarbon 41, 99–101.

Robinson, S.W., Thompson, G., 1981. Radiocarbon corrections for marine shell dates with application to southern Pacific Northwest coast prehistory. Syezis 14, 45–57.

Rowe, J.H., 1965. An interpretation of radiocarbon measurement on archaeological simples from Peru. compilers In: Chatters, R.M., Olson, E.A. (Eds.), Proceedings of the 6th International Conference Radiocarbon and Tritium. Clearinghouse for Federal Scientific and Technical Information, Springfield (Virginia, pp. 187–198.

Schiffer, M.B., 1986. Radiocarbon dating and the "old wood" problem: the case of the Hokokam chronology. Journal of Archaeological Science 13, 13–30.

Schneider, W., Fuenzalida, R., Rodrıguez-Rubio, E., Garces-Vargas, J., 2003. Characteristics and formation of Eastern South Pacific Intermediate Water. Geophysical Research Letters 30 (11), 1581 doi:10.1029/2003GL017086, 200.

Schwerdtfeger, W., 1976. Climates of Central and South America. World Survey of Climatology 12.

Shackleton, N.J., Duplessy, J.C., Arnold, M., Maurice, P., Hall, M., Cartlidge, J., 1988. Radiocarbon age of the last glacial Pacific Deep Water. Nature 335, 708–711.

Sikes, E.L., Samson, C.R., Guilderson, T.P., Howard, W.R., 2000. Old radiocarbon ages in the southwest Pacific Ocean during the last glacial period and deglaciation. Nature 405, 555–559.

Southon, J.R., Nelson, D.E., Vogel, J.S.A., 1990. Record of past ocean-atmosphere radiocarbon difference from the northeast Pacific. Paleoceanography 5, 197–206.

Southon, J.R., Rodman, A., True, D., 1995. A comparison of marine and terrestrial radiocarbon ages from northern Chile. Radiocarbon 37, 389–393.

Strub, T., Mesías, J., Montecino, V., Rutllant, J., Salinas, S., 1998. Coastal ocean circulation off western South America. In: Robinson, Allan R., Brink, Kenneth H. (Eds.), The Sea, vol. 11, pp. 273–313.

Stuiver, M., Braziunas, T.F., 1993. Modeling atmospheric ^{14}C influences and 14C ages of marine samples to 10 000 B.C. Radiocarbon 35, 137–191.

Stuiver, M., Polach, H.A., 1977. A discussion and reporting of ^{14}C data. Radiocarbon 19, 355–363.

Stuiver, M., Reimer, P.J., 1993. Extended 14C database and revised CALIB radiocarbon calibration program. Radiocarbon 35, 215–230.

Stuiver, M., Pearson, G.W., Braziunas, T.F., 1986. Radiocarbon age calibration of marine samples back to 9000 cal yr BP. Radiocarbon 28, 980–1021.

Stuiver, M., Reimer, P.J., Braziunas, T.F., 1998. High-precision radiocarbon age calibration for terrestrial and marine samples. Radiocarbon 28, 980–1021.

Taylor, R.E., 1987. Radiocarbon dating: An archaeological perspective. Academic Press, New York.

Taylor, R.E., Berger, R., 1967. Radiocarbon content of marine shells from the Pacific coast of central and south America. Science 158, 1180–1182.

Toggweiler, J.R., Dixon, K., Broecker, W.S., 1991. The Peru upwelling and the ventilation of the South Pacific Thermocline. Journal of Geophysical Research 96 (C11), 20467–20497.

Torres, R., Turner, D.R., Rutllant, J., Sobrazo, M., Antezana, T., Gonzalez, H., 2002. CO2 outgassing off central Chile (31-30ºS) and northern Chile (24-23ºS) during austral summer 1997: the effect of wind intensity on the upwelling and ventilation of CO2-rich waters. Deep Sea Research I 49, 1413–1429.

Ulm, S., 2002. Marine and estuarine reservoir effects in central Queensland, Australia: Determination of ΔR values. Geoarchaeology 17, 319–348.

Van Beek, P., Reyss, J.-L., Paterne, M., Gersonde, R., van der Loeff, M.R., Kuhn, G., 2002. ^{226}Ra in barite: Absolute dating of Holocene Southern Ocean sediments and reconstruction of sea-surface reservoir ages. Geology 30, 731–734.

Vargas, G., Ortlieb, L., Pichon, J.J., Pujos, M., Bertaux, J., 2004. Sedimentary facies and high resolution primary production inferences from laminated diatomaceous sediments off northern Chile. Marine Geology 211, 79–99.

Vargas, G., Rutllant, J., Ortlieb, L., 2006. ENSO tropical-extratropical climate teleconnections and mechanisms for Holocene debris flows along the hyperarid coast of western South America (17º-24ºS). Earth and Planetary Sciences Letters 249, 467–483.

Veit, H., 1996. Southern Westerlies during the Holocene deduced from geomorphological studies in the Norte Chico, northern Chile (27-33ºS). Palaeogeography, Palaeoclimatology, Palaeoecology 123, 107–119.

Villagrán, C., Varela, J., 1990. Palynological evidence for increased aridity on the Central Chilean coast during the Holocene. Quaternary Research 34, 198–207.

Villa-Martínez, R., Villagrán, C., Jenny, B., 2003. The last 7500 cal yr B.P. of westerly rainfall in Central Chile inferred from a high-resolution pollen record from Laguna Aculeo (34°S). Quaternary Research 60, 284–293.